

Field measurements and non-linear prediction of wave celerity in the surf zone

M. Tissier^{a,*}, P. Bonneton^a, R. Almar^a, B. Castelle^a, N. Bonneton^a, A. Nahon^b

^a Université Bordeaux 1, CNRS, UMR 5805-EPOC, Talence, F-33405, France

^b LNEC, DHA-NEC, Av. do Brasil, 101-Lisbon, Portugal

ARTICLE INFO

Article history:

Available online 25 November 2010

Keywords:

Celerity predictors

Surf zone

Non-linearities

ABSTRACT

A good prediction of wave celerity in the surf zone is essential for wave propagation modelling in the nearshore. This paper is devoted to a study of wave celerity based on the analysis of data collected during the ECORS 2008 field experiment that took place at Truc Vert Beach, SW France. Here we analyze and quantify the effects of non-linearities and evaluate the predictive ability of several non-linear celerity predictors for high-energy wave conditions. The asymptotic behaviour of the different models for high values of the non-linearity parameter is investigated. Besides, comparisons with data show that the classic bore model is inappropriate for describing wave dynamics when approaching the swash zone. The influence of very low frequency pulsations of the wave-induced circulation on wave celerity is also discussed.

© 2010 Elsevier Masson SAS. All rights reserved.

1. Introduction

As waves propagate to shallower water, they become steeper and higher until they break. Broken waves keep propagating shoreward through the surf zone. Immediately after breaking, the wave shape evolves rapidly. Thereafter, waves evolve more slowly as they reorganize into quasi-periodic bore-like waves in the inner surf zone. Very steep fronts are observed, which give to waves a typical saw-tooth profile (see Fig. 1). Waves finally end up in the swash zone where the run-up starts. Thus, waves are increasingly non-linear while they propagate shoreward. This high complexity explains why some basic wave parameters, such as wave celerity, are still not accurately described inside the surf zone.

A good prediction of broken wave celerity, c_b , is essential, as it is a key parameter in nearshore wave propagation models. In phase-averaged wave propagation models, the mass flux, energy flux and wave dissipation depend on c_b . The celerity predictors used in these models rely on the assumption of a given (fixed) wave shape, or at least a slowly variable one, whereas in the surf zone the wave shape can evolve quickly. For instance, broken wave celerity is often predicted using the linear shallow water theory, with the phase speed $c_\varphi \approx (gd)^{1/2}$ (where d is the local water depth), or the classic non-linear bore model [1]. In time-dependent Boussinesq-type models, a parameterization of c_b is also generally

required: rough approximations such as $c_b = 1.3(gd)^{1/2}$ are often used (see [2]).

In situ studies of wave celerity are also important for the development of remote sensing techniques (see for instance [3–5]). For example, wave celerity can be computed over a large area from video imaging, and subsequently the bathymetry and its evolution can be estimated through depth-inversion techniques. The accuracy of the results is directly dependent on the knowledge of a good functional relationship between wave celerity and water depth. This accuracy has been found to significantly degrade in the surf zone. Most depth-inversion techniques rely on the linear dispersion relation $c_\varphi = \left(\frac{g}{k} \tanh(kd)\right)^{1/2}$. Holland [3] investigated the validity of this dispersion relation for depth inversion. Using field data, he showed that the linear dispersion relation was commonly leading to depth errors of over 50% inside the surf zone, whereas the average depth estimation error was 3–9% outside the surf zone.

Despite a clear need for validation of the different celerity predictors, only a few works have been devoted to the experimental study of wave celerity. Catalán and Haller [4] compared the predictions of several linear and non-linear models with laboratory data, in application to depth inversion. Concerning field data, a key study was performed by Thornton and Guza [6]. Using a shore-normal transect of pressure and current sensors, they computed celerity spectra, $c_\varphi(\nu)$, from pairs of adjacent sensors, for $d < 7$ m. They observed that the celerities were almost invariant with frequency inside the surf zone, demonstrating that non-linear effects were prevailing over dispersive effects. Thus, the study of wave celerity through the computation of c_φ at different frequencies is not relevant inside the surf zone. In this paper, we analyze broken wave celerity, defining it as the wave front speed. An adequate method

* Corresponding author.

E-mail addresses: m.tissier@epoc.u-bordeaux1.fr (M. Tissier), p.bonneton@epoc.u-bordeaux1.fr (P. Bonneton), r.almar@epoc.u-bordeaux1.fr (R. Almar), b.castelle@epoc.u-bordeaux1.fr (B. Castelle), n.bonneton@epoc.u-bordeaux1.fr (N. Bonneton), anahon@lnec.pt (A. Nahon).

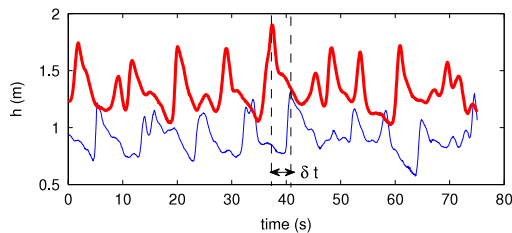


Fig. 1. Example of time series of water depths at two synchronized pressure sensors (the offshore sensor is the thick line).

for its computation is presented in Section 2. This study is based on the analysis of an extensive in situ data set collected during the ECORS Truc Vert 2008 field experiment (Section 3). The influence of wave non-linearities on c_b is examined, in particular for high energy wave events. Then, we evaluate the predictive ability of several non-linear celerity models (Section 4), and finally, the influence of very low frequency pulsations of the circulation on wave celerity is discussed (Section 5). Conclusions are stated in Section 6.

2. Field data and methods

2.1. Description of the study area

The study is based on data collected during the ECORS (SHOM-DGA) field experiment [7], a 6-week period of international fieldwork, carried out in March–April 2008 at Truc Vert Beach. This sandy beach is located on the southern part of the French Atlantic coastline, at approximately 10 km north of the Cap Ferret spit at the mouth of the Arcachon Lagoon.

This double-barred beach has a fairly mild slope of about 3% and typically exhibits an inner bar and rip system in the intertidal domain (see [8]). However, the inner-bar geometry was reasonably

alongshore uniform throughout the experiment as a result of quasi-persistent high-energy conditions and high offshore wave angle to the shore. A detailed description of the inner bar evolution is given in [9]. During the field experiment, the tidal range ranged from 2 m to about 4 m, allowing instruments to be deployed safely at low tide while measurements were obtained from about mid tide to high tide.

The offshore wave characteristics were given by a waverider buoy deployed offshore of the study area in 54 m water depth. A very wide variety of incoming swell conditions were encountered during the deployments (see the grey areas in Fig. 2), from small (significant wave height $H_{1/3} = 1$ m) to very large waves ($H_{1/3} = 8$ m), and significant wave periods mostly varying from 6 to 14 s. In particular, four storm events were recorded during the experiment ($H_{1/3} > 4$ m), including a 10-year return storm with H_{\max} larger than 10 m.

2.2. Instrument deployment

Synchronized pressure sensor lines were set up in the cross-shore direction. Several cross-shore transects were deployed consecutively at different locations. Each transect was made up of an acoustic Doppler velocimeter (ADV) in a central location, surrounded by two pressure sensors synchronized in time with the ADV, separated by about 15 m. Data were acquired at a sample rate of 16 Hz.

Instruments were deployed in fairly alongshore-uniform parts of the beach (see Fig. 3). While well-developed inner bar and rip morphology typically results in ubiquitous intense rip current circulations along this section of coastline [10], rip channels only barely form at the end of the experiment during low-energy wave conditions (see [9]), that is, when concurrent broken-wave celerity measurements were not performed. When celerity measurements were performed, rip current circulations were quasi-non-existent because of both the alongshore-uniform beach geometry

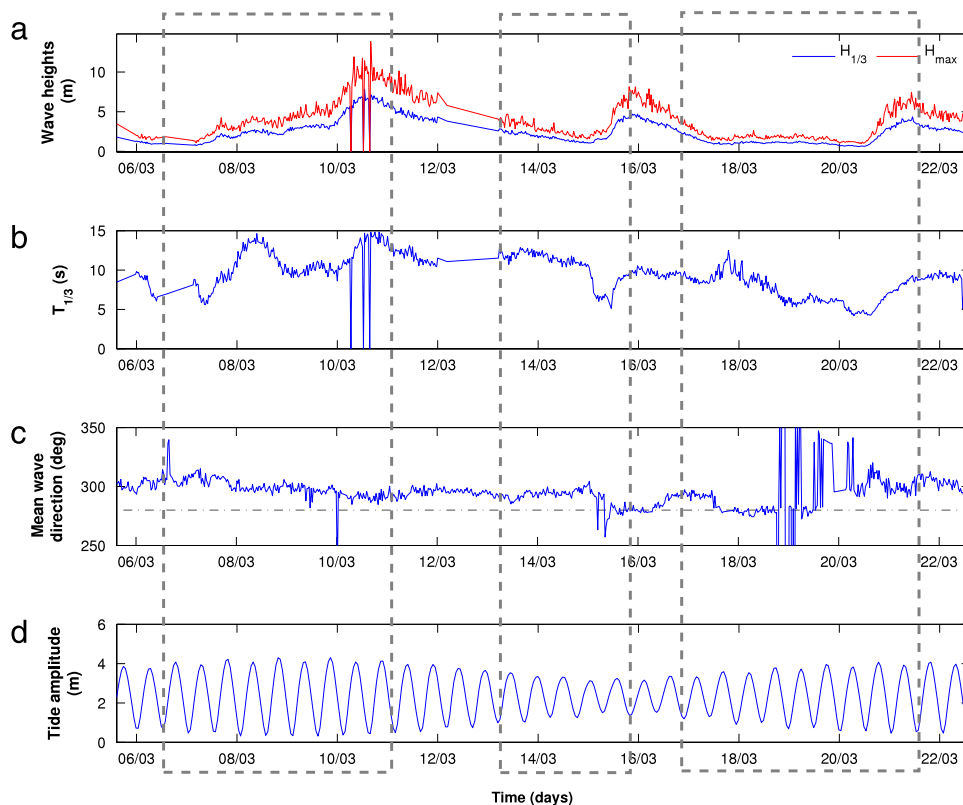


Fig. 2. Time series of wave and tide conditions offshore of the study area (at 54 m depth). (a) Significant and maximum wave heights (m). (b) Significant period (s). (c) Mean wave direction (\circ), (—): normal incidence to the shore. (d) Tide amplitude (m). The dashed frames mark the successive instrument deployments.

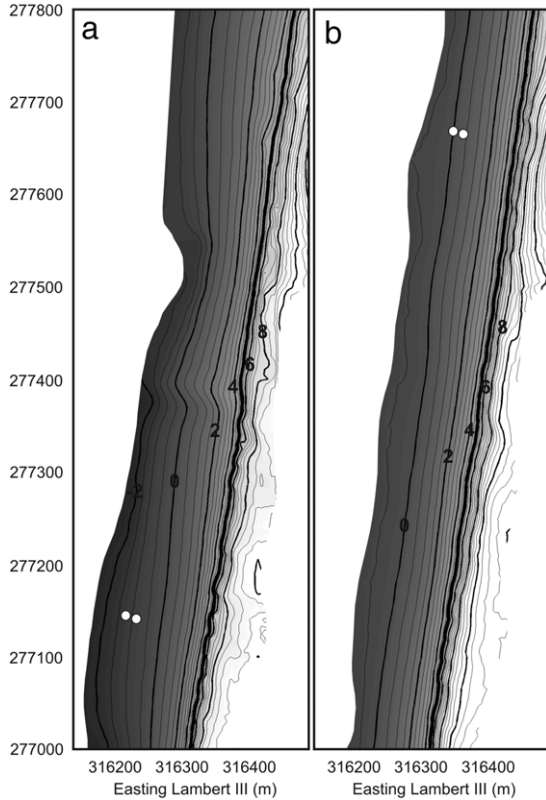


Fig. 3. (a) Location of the two pressure sensors (white circles) deployed from 6 March to 11 March 2008 superimposed on the beach morphology surveyed on 9 March. (b) Location of the two pressure sensors (white circles) deployed from 13 March to 21 March 2008 superimposed on the beach morphology surveyed on 14 March. Note that in both panels the ADVs are located between the pressure sensors.

and the high offshore wave angle to the shore. Therefore cross-shore and longshore currents are assumed to have been rather alongshore uniform during most of the experiment, which means that wave-current refraction was not significant. Moreover, the tide-induced currents are extremely weak along this section of the coastline [11], and therefore do not affect the wave directionality. Thus, while propagating shoreward, the wave direction is mainly affected by bathymetric refraction. Considering the fairly alongshore-uniform beach morphology at the deployment area, we assume that when the waves reached the sensors they were propagating nearly normally to the beach: we estimate that the wave angle to the shore was less than 10° . The celerity measured at our transects is the cross-shore component of the celerity. However, for an incidence angle smaller than 10° , the measured celerity is a good estimation of the total celerity, with less than 2% error. In this study, we neglect wave obliquity effects and we consider the measured celerity as the total wave celerity. Celerity data was recorded during 23 high tides, corresponding to about 140 h.

2.3. Computation of absolute and relative wave celerity

In this study, the broken wave celerity is computed in the following way:

$$c_b = \frac{dx_b}{dt} \approx \frac{\delta D}{\delta t}, \quad (1)$$

where x_b is the cross-shore position of the wave front, δD the distance which separates the sensors and δt the time lag between the signals recorded by the two pressure sensors (see Fig. 1).

From a practical point of view, δt was computed with a cross-correlation between two different sensor time series. Thus, we do

not determine the time lag for a given wave, but for a set of several consecutive waves, and consider c_b as an estimation of the mean celerity of the wave fronts during a few minutes (averaging over 10 or 3 min in this study). The time lag δt is determined with a precision of $\pm 1/f_{\text{sampl}}$ s, with $f_{\text{sampl}} = 16$ Hz the sampling rate of the sensors, leading to a maximum error of 2% on the measure of celerity (for $\delta D = 15$ m).

As the wave celerity can evolve quickly within the surf zone, the choice of δD is of significant importance. In order to test our spatial resolution, we performed some computations of wave celerities considering a distance two times shorter. These celerities were consistent with those computed for $\delta D = 15$ m with less than 2% error.

The sensitivity of the cross-correlation method to low-frequency and high-frequency components of the signal was investigated. Comparisons between the celerity obtained with and without prior high-frequency filtering of the signal were performed for 250 values, with a cut-off frequency $f_c = 1/3$ Hz. The difference was negligible (about 1% in total). Similar results were obtained with prior suppression of low-frequency oscillations ($f_c = 1/25$ Hz).

The measured wave celerity is relative to the beach: it is an absolute celerity, c_a . In the case of a current superimposed on the waves, there is a shift in the celerity that should be taken into account, since the different theories give a celerity relative to the water c_r . We have to consider the effects of the cross-shore current, generally vertically sheared, on wave celerity. Kirby and Chen [12] showed that for a vertically variable current $U(z)$ such as $|U/c| < O(1)$ we have $c_a = c_r + U_e$ with, in shallow water,

$$U_e = \frac{1}{h} \int_{-h}^0 U(z) dz. \quad (2)$$

The cross-shore current was measured at a single elevation by the ADV, close to the bottom (30–50 cm from the sand bed). For most of the data (22 tides of the 23), the 10 min averaged cross-shore velocities measured by the ADV, U_m , were such as $|U_m/c_b| < 0.05$. Moreover, they were offshore directed: they correspond to undertow-type currents. Several studies have shown that the intensity of this type of current varies significantly vertically, and generally reaches its maximum close to the seabed (see for instance [13,14]), that is, in the vicinity of the location of our current meters. The depth-integrated and time-integrated velocity $|U_e|$ is therefore smaller than $|U_m|$. We estimate that U_e represents at the most 2.5% of c_b , which is of the order of magnitude of the errors on the computation of c_b . U_e is neglected for those tides, i.e. the measured celerity is representative of the relative celerity. The remaining data (called record 13) will be studied separately in Section 3.

On the whole, we estimate that c_b is a good estimation of the broken wave celerity, with less than 3% error.

The present work is exclusively devoted to the study of wave celerity in the surf zone. As the location of the surf zone can vary, depending on the tide and incoming wave heights, the same instruments can be located inside the surf zone at a given time, and in the shoaling zone later. The 10 min (or 3 min) long records corresponding to non-breaking waves are therefore identified and removed from the dataset. For some of the deployments, video images of the area were recorded, and thanks to time-stack analysis (see [5] for details), the width and position of the surf zone can be precisely determined throughout the experiment. When this information is not available, we estimate the difference of energy between the two sensors using the linear theory in order to identify when breaking occurred.

After calibration of the sensors, statistic wave characteristics (the mean wave heights, period and water level) are computed for the pressure sensors using a wave-by-wave analysis (see [15] for the method).

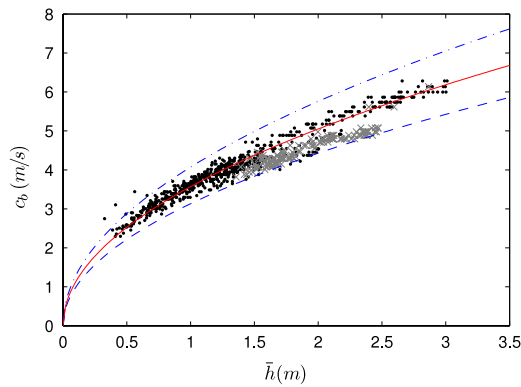


Fig. 4. c_b as a function of \bar{h} . Data inside the surf zone (\bullet), outside the surf zone (grey \times), $(g\bar{h})^{1/2}$ (---), $1.3(g\bar{h})^{1/2}$ (- · -), $1.14(g\bar{h})^{1/2}$ (—).

3. Analysis of experimental results

The results presented in this section are based on celerities calculated by cross-correlation between 10 min long signals, which represent a data set of 707 values of celerity in the surf zone.

In the surf zone, the wave dynamics are mainly controlled by two non-dimensional parameters: $\epsilon = H/d$ and $\mu = d/L$, where H is the wave height, d the characteristic water depth (from a practical point of view, d is estimated by the mean water depth \bar{h}) and L the wavelength. The parameter μ quantifies the frequency dispersion effects, and ϵ quantifies the non-linear effects. For our dataset, $\mu \sim 0.01$ – 0.07 , while ϵ can be $O(1)$.

Fig. 4 shows c_b as a function of the mean water level \bar{h} . The dashed line is the linear approximation in shallow water ($\mu \ll 1$): $c_\phi = (g\bar{h})^{1/2}$. To first order, the linear theory gives a good description of the measured celerities, despite an overall underestimation. Considering the dispersive effects, with the exact linear phase velocity $c_\phi = (\frac{g}{k} \tanh(k\bar{h}))^{1/2}$, does not improve the prediction, since it leads to an even larger underestimation of c_b . For the surf zone data, the quadratic error given by the linear theory is $R_{\text{rms}} = 12.8\%$. The empirical modification of the linear theory $1.3(g\bar{h})^{1/2}$, arisen from laboratory observations (see [16]), and commonly used in nearshore propagation models (for instance [2]), does not give a better prediction as $R_{\text{rms}} = 15.3\%$. For our data set, the best predictor in the form $a(g\bar{h})^{1/2}$ is obtained for $a = 1.14$ (see the plain line in Fig. 4), with $R_{\text{rms}} = 4.8\%$.

In previous field data studies (see for instance [6], and more recently [3]), a strong correlation between the error given by the linear theory and the broken-wave heights was observed. In particular, Holland [3] emphasized the importance of accounting for wave amplitude in the calculation of wave celerity with respect to depth inversion. The amplitude dependence of c_b is studied in detail in the following part of the paper, which includes results for highly non-linear waves.

Finite-amplitude effects can be quantified by the non-linearity parameter ϵ , calculated here for 10 min periods. The value of ϵ depends significantly on the location inside the surf zone. In the inner surf zone, ϵ remains close to a constant value of about 0.4, while it increases quickly when the wave approaches the swash zone (small \bar{h}). These variations are consistent with those observed in previous field studies, in particular with those in [17], concerning a previous experiment at the same study area.

Fig. 5 shows the measured celerities normalized by the linear approximation in shallow water (dots) as a function of the non-linearity parameter ϵ . In order to study the behaviour for strong non-linearities, a second data processing was specifically performed for the smallest water depth recorded. This second dataset is represented by crosses. These parts of the signal were not used at first because both sensors were not always

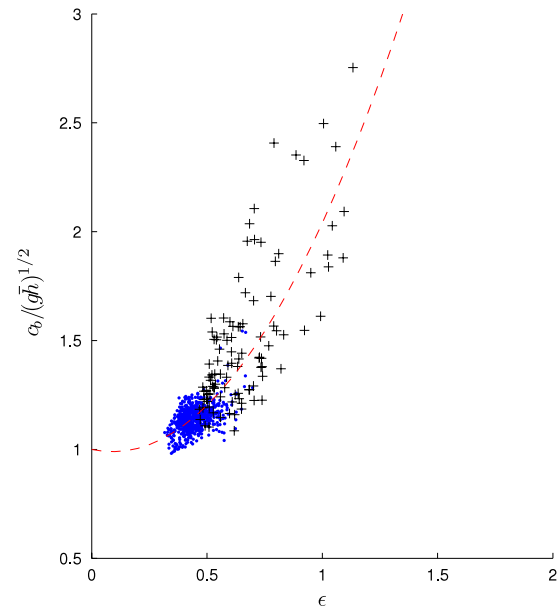


Fig. 5. $c_b/(g\bar{h})^{1/2}$ as a function of ϵ . (\cdot): data inside the surf zone (first data processing). (\times): data obtained by a second specific processing for small water depth. (---): polynomial fit of the data ($c_b/(g\bar{h})^{1/2} = 0.13\epsilon^2 - 0.23\epsilon + 1$).

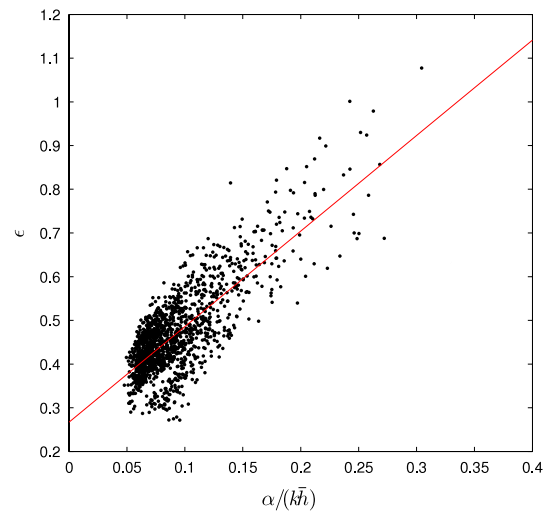


Fig. 6. ϵ as a function of $\alpha/(k\bar{h})$. (red —): linear fit of the data ($\epsilon = 2.19\alpha/(k\bar{h}) + 0.27$).

totally submerged. In this case, the way to determine wave characteristics implies some approximations and so is presumably less accurate. In particular, h is approximated using the water depth measured by the most submerged sensor corrected by the local beach slope to estimate its value between the sensors, considering that set-up effects are not significant over the considered distance. In order to determine ϵ at the most onshore sensor, we follow the analysis of [18–20], who found a positive linear dependence of ϵ on the normalized slope $\alpha/(k\bar{h})$ (where α is the local beach slope). ϵ is then calculated using a linear relationship between ϵ and $\alpha/(k\bar{h})$ deduced from the initial dataset (see the red line in Fig. 6). Hereafter, we call *Data1* the first part of the dataset (\cdot) in Fig. 5, where wave characteristics are directly computed from measurements. The whole dataset, including values computed from the second data processing (\times), is called *Data2*.

If the accuracy of the computation of c_b is not significantly deteriorated for this second part of the dataset, the computation of the highest values of ϵ is presumably less accurate since they

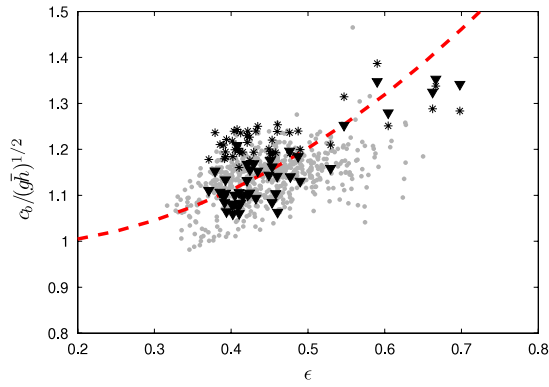


Fig. 7. Effect of the mean cross-shore current, $c_b/(g\bar{h})^{1/2}$ as a function of ϵ , for the whole data set in grey, and for record number 13 in black, without (\blacktriangledown) and with ($*$) previous subtraction of the mean cross-shore current. (red - - -): polynomial fit of the data defined in Fig. 5.

are determined using a rough empirical relationship. However, it clearly appears that the difference between measured celerities and linear predictions increases significantly for high values of ϵ , with c_b exceeding up to 2.5 times the linear prediction. This demonstrates that a predictor such as $a(g\bar{h})^{1/2}$ is no longer accurate when considering high values of ϵ .

The data corresponding to tide 13 have been treated separately, since they correspond to a higher intensity of the measured cross-shore current U_m (after averaging over 10 min). U_m was representing up to 15% of the c_b . Moreover, the currents were onshore directed during this particular event, as the measurements were concurrent to the establishment of a rip current circulation. The current meter was located in the vicinity of the onshore component of the wave-driven circulation cell. Wave-driven rip current circulations are known to be nearly depth uniform except in the rip head and the feeder currents [21]. Therefore, Eq. (2) reads $U_e \approx U_m$, and implies that the effect of the mean current cannot be neglected any longer. Absolute ($*$) and relative (\blacktriangledown) normalized celerities are plotted in Fig. 7. It shows that, accounting for currents for this specific tide, the wave celerities are getting closer to the polynomial approximation previously defined in Fig. 5 ($R_{\text{rms}} = 3.9\%$ instead of 7.1%).

4. Evaluation of the predictive abilities of several non-linear celerity models

4.1. Global comparison

It has been shown in Section 3 that we have to consider non-linear predictors to obtain a more accurate description of broken wave celerity. An exhaustive description of the different celerity models is given in [4]. In the present study, we focus on the evaluation of the three most representative non-linear predictors. The solitary wave model, a constant form solution of the Boussinesq equations, is historically one of the first models used to describe non-linear behaviour. Although it has not been formally derived for broken waves, it has been quite commonly used to describe wave celerity in shallow water. In this case, the wave celerity is given by

$$c_b = (g\bar{h}(1 + \epsilon))^{1/2}. \quad (3)$$

It has been found in previous studies that this predictor tends to overestimate broken wave celerities (see [6] for instance).

The bore model, developed by Svendsen et al. [1], is based on the classical analogy between a broken wave and a hydraulic jump. The wave front celerity is derived from mass and momentum conservation across the wave front:

$$c_b = \left(\frac{gh_1 h_2 (h_1 + h_2)}{2\bar{h}^2} \right)^{1/2}, \quad (4)$$

with h_1 and h_2 the water depths respectively ahead of and behind the wave front. Most phase-averaged wave models are based on this expression of c_b .

Bonneton, in [22], proposed a generalization of the bore model using the Saint-Venant shock theory (called the shock model hereafter). The wave fronts are approximated here using a less restrictive hypothesis, by introducing discontinuities satisfying appropriate shock conditions. In particular, contrary to the classical bore model, the wave shape in this model does not have to be constant. The broken-wave celerity is given by

$$c_b = -2(g\bar{h})^{1/2} + 2(gh_1)^{1/2} + \left(\frac{gh_2}{2h_1} (h_1 + h_2) \right)^{1/2}. \quad (5)$$

For the two last models, wave asymmetry is taken into account with the introduction of h_1 and h_2 . We define a new non-dimensional parameter representative of wave asymmetry: $\beta = \zeta_c/H$, with $\zeta_c = h_2 - \bar{h}$ the wave crest elevation.

For *Data1*, we obtain the following errors for the 10 min averaged celerities: 6.7% for the shock model, 7.2% for the solitary model and 9.9% for the bore model. These results are illustrated in Fig. 8 (\cdot), where the wave celerity predictions are plotted as a function of the measurements. Considering the whole dataset *Data2*, the shock model gives a global error of 11.3%, while the solitary wave predictor gives an error of 9.9% and the bore model an error of 14.9%. The three non-linear models give good predictions, but the ability of the solitary wave model and the shock model to predict the broken-wave celerity is slightly better. We have to notice that the 10 min averaging tends to smooth the variations of the wave characteristics. In particular, the dimensionless parameter β is almost constant when averaged over 10 min, whereas the scattering of the values is more important when we consider shorter times (not shown here). It is interesting to compare the ability of these two models to reproduce higher-frequency oscillations. For 3 min long computations, i.e. with a dataset of 2286 values in the surf zone (corresponding to *Data1*), we find $R_{\text{rms}} = 7.0\%$ for the shock model, and 8.0% for the solitary wave model. The shock model gives a slightly better prediction of wave celerity than the solitary wave model when considering high-frequency variations of c_b .

4.2. Asymptotic behaviour of the models for high values of the non-linearity parameter

The different models have been compared for the whole dataset, but it is important to point out that a large majority of the measurements were acquired in the inner surf zone, i.e., for $\epsilon \sim 0.4$ – 0.5 . In the present section, efforts are concentrated on evaluating how the accuracy of the models varies as a function of non-linearities, based on the analysis of the 10 min averaged celerities.

Wave celerities can be rewritten as a function of ϵ and β only in the following forms:

$$\frac{c_b}{(g\bar{h})^{1/2}} = [(1 + (\beta - 1)\epsilon)(1 + \beta\epsilon)(1 + (\beta - 1/2)\epsilon)]^{1/2} \quad (6)$$

for the bore model, and

$$\frac{c_b}{(g\bar{h})^{1/2}} = -2 + 2(1 + (\beta - 1)\epsilon)^{1/2} + \left[\frac{(1 + \beta\epsilon)(1 + (\beta - 1/2)\epsilon)}{1 + (\beta - 1)\epsilon} \right]^{1/2} \quad (7)$$

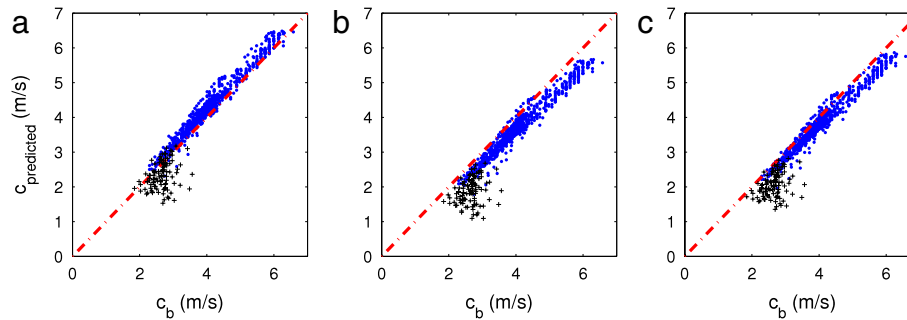


Fig. 8. Comparisons of predictions versus measurements for the three models for 10 min averaging. (a) Solitary model ($R_{rms} = 7.2\%$). (b) Bore model (9.9%). (c) Shock model (6.7%). (·): first data processing. (+): data obtained by a second specific processing for small water depth. (· - ·): $c_{predicted} = c_b$.

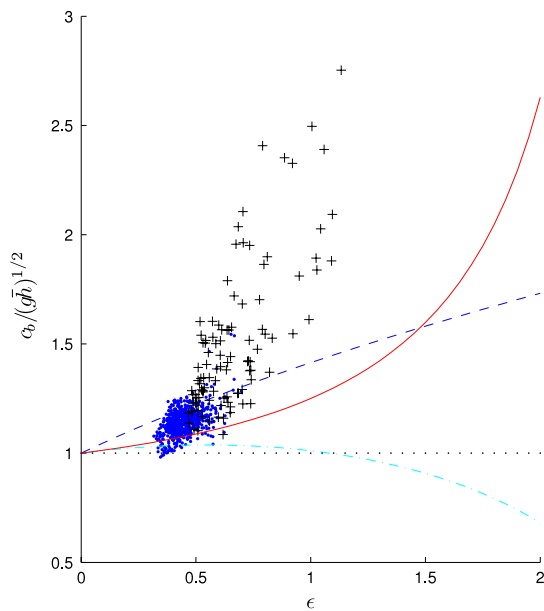


Fig. 9. $c_b/(g\bar{h})^{1/2}$ versus ϵ . Linear model: (· · ·). Shock model: (—). Solitary wave model: (---). Bore model (· - ·).

for the shock model. The solitary wave celerity model can also be written under the same form, as a function of ϵ only (see relation (3)). As β is almost constant while considering 10 min computations, we set β equal to its mean value and we compare the evolution of $c_b/(g\bar{h})^{1/2}$ versus ϵ for the three models (see the curves in Fig. 9). In the inner surf zone, the behaviour of the shock and bore models is similar: they both tend to slightly underestimate the celerities, in contrast to the solitary wave model, which overestimates them. It is in the vicinity of the swash zone that the differences become striking: only the bore model predicts a decrease of the rations $c_b/(g\bar{h})^{1/2}$ for strong nonlinearities, in opposition to the observations. Thus, the bore celerity

model, which is the most commonly used predictor of c_b , appears to be inappropriate for describing the dynamics for the shallowest water depths. The shock and solitary wave models both predict an increase of the normalized celerity, but neither of them seems to follow the tendency observed in the data. It is noteworthy that only the shock model predicts normalized celerities of the same order of magnitude as the measurements.

5. Influence of very low frequency oscillations of the wave-induced currents on wave celerity

Wave breaking over complex bathymetries as observed on the inner bar at Truc Vert beach induces the generation of circulation cells which are non-stationary. Very low frequency (VLF) pulsations can be observed in wave-induced currents, i.e., oscillations at significantly lower frequencies than the infragravity waves ($f < 0.04$ Hz). Recently, several studies have been devoted to the observation or the modelling of these VLF motions [23–27].

In particular, [26,27] have recently emphasized the strong spatial variability of the intensity of these VLF motions, in both cross-shore and longshore directions. For instance, they are more intense in the rip neck than over the bars, and are mostly contained within the surf zone. The authors pointed out the need to investigate in more detail VLF spatial variability in topographically controlled rip current systems.

For most of our deployments, we identified slow oscillations in the cross-shore current (after a 3 min running mean averaging) at the VLF timescales. For instance, Fig. 10 shows 10–15 min oscillations of the mean cross-shore currents, with an amplitude up to 20 cm/s.

As the measured wave celerity can be written as $c_b = c_r + U_e$ (see Eq. (2)), the VLF oscillations of the cross-shore current should induce VLF oscillations of c_b , if c_b is averaged over short enough durations. Fig. 10 compares the 3 min averaged cross-shore current with the mean wave celerities computed on 3 min long periods, with a 1 min shift between two consecutive computations. Both signals oscillate with similar amplitude and frequency. Although we cannot explain the phase difference observed in some parts of

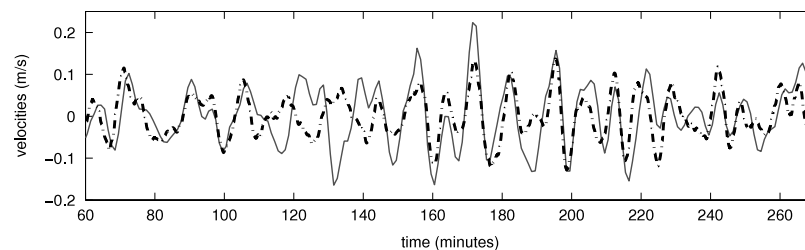


Fig. 10. Evidence of correlation between VLF oscillations of the cross-shore current and wave celerity. (—): cross-shore current after 3 min running averaging. (· - ·): oscillations of the 3 min averaged wave celerity. For both signals, the mean value has been removed.

the signal, it is clear that VLF oscillations of the cross-shore current significantly affect the wave celerity fluctuations.

Observation of wave celerity is then an indirect way to characterize very low frequency instationarities of the wave-induced currents. As the wave celerity can be estimated from video imaging over large areas [5], very low frequency motions may be quantified through remote sensing techniques. Considering the difficulties and expense of collecting data by in situ means, this way of studying VLF motions could be a very interesting alternative to in situ studies.

6. Conclusion

The influence of non-linearities on wave celerity in the surf zone has been quantified. In particular, we found an asymptotic behaviour of the normalized wave celerity $c_b/(gh)^{1/2}$ for high values of $\epsilon = H/d$. Comparisons with the predictions given by the three most representative non-linear celerity predictors have been performed. The non-linear models give relatively accurate predictions in the surf zone for $\epsilon \sim 0.4$ – 0.5 , with rms differences less than 10%. However, their predictions are less accurate when the waves are approaching the swash zone, i.e., when we consider high values of the non-linear parameter ϵ . In particular, the classical non-linear bore model, which is the most commonly used predictor in nearshore wave propagation models, is inappropriate for describing the wave dynamics in the vicinity of the swash zone. Contrary to the other non-linear models, it predicts a decrease of $c_b/(gh)^{1/2}$ with increasing ϵ .

The observation of VLF variations in wave front celerity, correlated with cross-shore current VLF variations, opens up new perspectives concerning the study of VLF motions over a wide spatial area. We speculate that video imagery may be successful in mapping VLF motions from wave celerity to investigate spatial variability in VLF motions at the scale of the beach in detail.

This work is based on an unique dataset inside the surf zone, including data for very shallow water and very strong non-linearities. Broken wave celerities have been measured over a very wide range of incoming wave conditions, including some severe storms. If complemented by data collected on beaches of different morphologies, this dataset could be used as a reference for the parameterization of broken wave celerity for wave propagation models in the nearshore.

Acknowledgements

The authors are grateful for all the financial support of the field experiment, in particular the SHOM-DGA, in the framework of the ECORS project. The authors are also grateful to all the people involved in this experiment. In particular, we would like to thank J.-P. Parisot for GPS positioning and topography, as well as P. Bretel for the instrument deployment. The authors would also like to acknowledge additional financial and scientific support of the French INSU - CNRS (Institut National des Sciences de l'Univers - Centre National de la Recherche Scientifique) program IDAO ("Interactions et Dynamique de l'Atmosphère et de l'Océan"). The Ph.D. thesis work of M. Tissier is funded by MISEEVA (ANR).

References

- [1] I.A. Svendsen, P.A. Madsen, J.B. Hansen, Wave characteristics in the surf zone, *Proc. Int. Conf. on Coast. Eng., ASCE 1* (1978) 520–539.
- [2] H. Schäffer, P. Madsen, R. Deigaard, A Boussinesq model for waves breaking in shallow water, *Coastal Eng.* 20 (3–4) (1993) 185–202.
- [3] T.K. Holland, Application of the linear dispersion relation with respect to depth inversion and remotely sensed imagery, *IEEE Trans. Geosci. Remote Sens.* 39 (9) (2001) 2060–2072.
- [4] P.A. Catalán, M.C. Haller, Remote sensing of breaking wave phase speeds with application to non-linear depth inversions, *Coast. Eng.* 55 (1) (2008) 93–111.
- [5] R. Almar, P. Bonneton, N. Sénéchal, D.A. Roelvink, Wave celerity from video imaging: a new method, *Proc. Int. Conf. Coast. Eng., ASCE 1* (2008) 661–673.
- [6] E.B. Thornton, R.T. Guza, Energy saturation and phase speeds measured on a natural beach, *J. Geophys. Res.* 87 (C12) (1982) 9499–9508.
- [7] N. Sénéchal, S. Abadie, F. Ardhuin, E. Gallagher, J.H.M. MacMahan, G. Masselink, H. Michallet, Ad J.H.M. Reniers, B.G. Ruessink, P.E. Russell, D. Sous, I.L. Turner, P. Bonneton, S. Bujan, S. Capo, R. Certain, T. Garland, R. Pedreros, The ECORS-Truc Vert'08 field beach experiment: Presentation of a three-dimensional morphologic system in a macro-tidal environment during consecutive extreme storm conditions. *Ocean Dynam.* (2011) (submitted for publication).
- [8] B. Castelle, P. Bonneton, H. Dupuis, N. Senechal, Double bar beach dynamics on the high-energy meso-macrotidal French Aquitanian coast: a review, *Mar. Geol.* 245 (1–4) (2007) 141–159.
- [9] R. Almar, B. Castelle, B.G. Ruessink, N. Sénéchal, P. Bonneton, V. Marieu, Two- and three-dimensional double-sandbar system behaviour under intense wave forcing and a meso-macro tidal range, *Cont. Shelf Res.* 30 (2010) 781–792.
- [10] N. Bruneau, B. Castelle, P. Bonneton, R. Pedreros, R. Almar, N. Bonneton, P. Bretel, J.-P. Parisot, N. Sénéchal, Field observation of an evolving rip current on a meso-macrotidal well-developed inner bar and rip morphology, *Cont. Shelf Res.* 29 (2009) 1650–1662.
- [11] N. Bruneau, P. Bonneton, B. Castelle, R. Pedreros, Modeling of a high-energy rip current on a meso-macrotidal environment: a way to predict some rip current characteristics? *J. Geophys. Res.* (2011) (in correction).
- [12] J.T. Kirby, T.-M. Chen, Surface waves on vertically sheared flows: approximate dispersion relations, *J. Geophys. Res.* 94 (C1) (1989) 1013–1027.
- [13] F.C.K. Ting, J.T. Kirby, Observations of undertow and turbulence in a laboratory surfzone, *Coast. Eng.* 24 (1994) 51–80.
- [14] D.T. Cox, N. Kobayashi, Application of an undertow model to irregular waves on plane and barred beaches, *J. Coast. Res.* 14 (4) (1998) 1314–1324.
- [15] L. Hamm, Modélisation numérique bidimensionnelle de la propagation de la houle dans la zone de déferlement, PhD Thesis, Université de Grenoble 1, 1995 (in French).
- [16] M.J.F. Stive, Energy dissipation in waves breaking on gentle slopes, *Coast. Eng.* 8 (1984) 99–127.
- [17] N. Sénéchal, H. Dupuis, P. Bonneton, Preliminary hydrodynamic results of a field experiment on a barred beach, Truc Vert beach on October 2001, *Ocean Dynam.* 54 (3–4) (2004) 408–414.
- [18] B. Raubenheimer, R. Guza, S. Elgar, Wave transformation across the inner surf zone, *J. Geophys. Res.* 101 (C11) (1996) 25589–25597.
- [19] N. Sénéchal, H. Dupuis, P. Bonneton, H. Howa, R. Pedreros, Observation of irregular wave transformation in the surf zone over a gently sloping sandy beach on the French Atlantic coastline, *Oceanol. Acta* 324 (6) (2001) 545–556.
- [20] N. Sénéchal, P. Bonneton, H. Dupuis, V. Rey, Determination and impact of the characteristic wave period in wave energy dissipation in the surf zone, in: *Proceeding Coastal Dynamics*, 2005.
- [21] K.A. Hass, I.A. Svendsen, Laboratory measurements of the vertical structure of rip currents, *J. Geophys. Res.* 107 (C5) (2002) 15.1–15.20.
- [22] P. Bonneton, Wave celerity in the surf zone, *Proc. Int. Conf. Coast. Eng., ASCE 1* (2004) 392–401.
- [23] J. MacMahan, E.B. Thornton, A.J.H.M. Reniers, Rip current review, *J. Coast. Eng.* 53 (2–3) (2006) 191–208.
- [24] N. Bonneton, P. Bonneton, N. Sénéchal, B. Castelle, Very low frequency rip current pulsations during high-energy wave conditions on a meso-macro tidal beach, *Proc. Int. Conf. Coast. Eng., ASCE 1* (2006) 1087–1096.
- [25] B. Castelle, P. Bonneton, N. Sénéchal, H. Dupuis, R. Butel, D. Michel, Dynamics of wave-induced currents over a multi-barred beach on the Aquitanian coast, *Cont. Shelf Res.* 26 (1) (2006) 113–131.
- [26] A.J.H.M. Reniers, J.H. MacMahan, E.B. Thornton, T.P. Stanton, Modeling of very low frequency motions during RIPEX, *J. Geophys. Res.* 112 (C07013) (2007).
- [27] N. Bruneau, B. Castelle, P. Bonneton, R. Pedreros, Very Low Frequency motions of a rip current system: observations and modeling, *J. Coast. Res.* SI56 (2) (2009) 1731–1735.